Astron. Astrophys. 323, 943–952 (1997)

ASTRONOMY
AND
ASTROPHYSICS

Structure and kinematics of a protostar: mm-interferometry of L 1157

F. Gueth[1], **S. Guilloteau**[1], **A. Dutrey**[1], **and R. Bachiller**[2]

[1] Institut de Radio Astronomie Millimétrique, 300 rue de la Piscine, F-38406 Saint Martin d'Hères, France
[2] Observatorio Astronómico Nacional (IGN), Apartado 1143, E-28800 Alcalá de Henares (Madrid), Spain

Received 18 November 1996 / Accepted 18 December 1996

Abstract. We present high angular resolution (2.5″) interferometric images of ^{13}CO J = 1 → 0 , C^{18}O J = 1 → 0 , and λ 2.7 mm continuum emission around L1157-mm, a suspected protostar powering an energetic molecular outflow. The continuum emission consists in two distinct components. The Class 0 object L1157-mm is seen as a compact source of size $\leq$ 1″ (440 AU) and mass $\simeq 0.2\,M_{\odot}$, which is marginally resolved and elongated perpendicular to the outflow axis. In addition, spatially-extended low-level emission is observed and likely arises at the heated edges of the cavity excavated by the outflow in the surrounding envelope. Simple modelisation shows that such an interacting structure can explain the observed morphology and the spectral energy distribution of the source.

The line observations indicate that ^{13}CO mostly originates from the envelope and the limb-brightened edges of the outflow, whereas the C^{18}O emission is more directly associated with the compact continuum source. Weak evidence for rotation has been found. Comparison of the two line tracers shows proeminent redshifted self-absorption in the ^{13}CO spectrum which is very suggestive of infall motions. The infalling medium seems to be confined in a large (a few thousands AU) flattened structure.

These observations provide a quite detailed description of the structure of a Class 0 protostar, which appears to have a complex vicinity where the outflowing and accreting phenomena are closely linked together.

Key words: stars: formation – ISM: individual objects: L 1157 – ISM: jets and outflows – ISM: molecules – radio lines: ISM

1. Introduction

The spectacular outflow in L1157 has been recently studied in many molecular lines including CO (Umemoto et al. 1992), SiO (Mikami et al. 1992; Zhang et al. 1995), H_2 (Hodapp 1994; Davis & Eislöffel 1995), NH_3 (Bachiller et al. 1993; Tafalla & Bachiller 1995), and CH_3OH (Bachiller et al. 1995; Avery & Chiao 1996). The blueshifted lobe of the flow has been mapped at 3.5″ resolution in ^{12}CO J = 1 → 0 by Gueth et al. (1996) revealing the presence of well defined cavities which are likely to be created by the propagation of large bow-shocks in a highly-collimated jet emerging from a very young protostar/disk system. All the observations seem to indicate that the L1157 outflow is particularly young and energetic. However, in spite of the efforts devoted to the study of the molecular outflow, little is known about the source which drives it. Since outflow and infall motions seem to be closely linked processes from the very initial stages of star formation (e.g. Bachiller 1996; Bontemps et al. 1996), we expect the source driving the L1157 outflow to be a prime target in star formation studies.

From the available observations, we know that the L1157 outflow is driven by IRAS 20386+6751, a cold, extremely red, young stellar object of only $L_{\rm bol} \sim 11\,L_{\odot}$ (for an assumed distance of 440 pc). This young object – hereafter called "L1157-mm" – presents all the attributes of the Class 0 prostostars (André et al. 1993), including a strong flux density at mm wavelengths, dominated by thermal dust emission from the protostellar condensation. The 115 GHz continuum images at 3.5″ resolution obtained by Gueth et al. (1996) revealed that the compact source was surrounded by low-level emission which was found to be extended *along* the outflow axis. In this paper, we present interferometric continuum mapping of the vicinity of L1157-mm with higher resolution and sensitivity. In addition, in order to investigate the kinematics of the dense gas around L1157-mm, we have mapped the source in the ^{13}CO and C^{18}O J = 1 → 0 lines. Such observations are important to study the possible gravitational infall motions which are expected to take place in such a young source.

2. Observations

The interferometric observations were carried out between November 1994 and March 1995 with the IRAM interferometer at Plateau de Bure (Guilloteau et al. 1992). Four configurations of the four antenna array were used, with baselines extending up to 290 m. The antennas were equipped with cooled SIS receivers with typical SSB system temperatures of about 250 K at the ob-

Send offprint requests to: F. Gueth

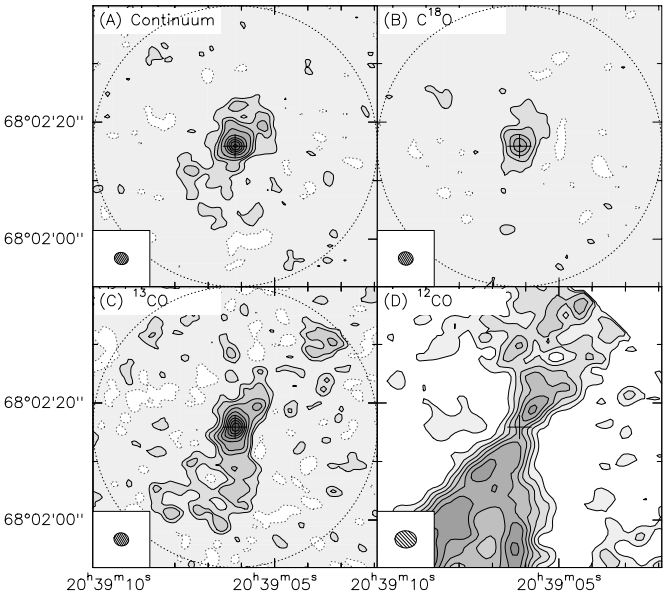

Fig. 1. a λ 2.7 mm continuum emission towards L1157. Contour values are -1, 1, 2, 3 and then 5 to 30 by step of 5 mJy/beam. **b** Integrated $C^{18}O$ J = 1 → 0 emission (over a 1.3 km.s^{-1} wide interval). Contours are -35, 35, 70, 140, 210, and 280 mJy.km.s^{-1}/beam. **c** Integrated ^{13}CO J = 1 → 0 emission (over a 3.2 km.s^{-1} wide interval). Contours are -35, 35, 70 to 560 by 70 mJy.km.s^{-1}/beam. In **a**, **b** and **c**, the clean beam is $2.4'' \times 2.1''$ at PA = 75°, and is drawn in the lower left corner. The half power primary beam of the interferometer is indicated as a dashed circle. **d** Integrated intensity of the ^{12}CO J = 1 → 0 emission (adapted from Gueth et al. 1996). Contours are 0.75 to 7.5 by 0.75 Jy.km.s^{-1}/beam. The beam size is $3.6'' \times 3''$. This map is actually a mosaic: the sharp edge in the upper right is due to the truncation that occurs in the reconstruction process of the mosaics.

serving frequency. To observe the ^{13}CO and $C^{18}O$ J = 1 → 0 lines, two correlator units were configured to give 256 channels of 0.078 MHz separation (0.21 km.s^{-1} at 110 GHz). The remaining units were configured in broad-band mode to provide the continuum data. Summing upper and lower sideband, this implies a total bandwith of 2×500 MHz. Phase calibration was achieved by observations of 2021+614, which is close in the sky to L 1157. Typical rms phase noise was better than 25°. Such phase noise introduces position errors smaller than $0.3''$. The bandpass of the receivers were calibrated by observations of 3C273, 3C454.3 or 2013+370. Variations in receiver gain and atmospheric opacity were corrected by frequent measurements of a chopper wheel at ambient temperature. To correct for decorrelation due to phase noise, amplitude calibration was also done relative to 2021+614, whose flux (0.35 Jy) was determined relative to 3C273, 3C454.3 and 2013+370 (the flux densities of these quasars were monitored against planets at the IRAM interferometer and 30-m telescopes).

We also obtained ^{13}CO J = 1 → 0 and J = 2 → 1 single-dish data in June 1995 at the IRAM 30-m telescope. SIS mixers with high sideband rejection (30 dB) provided system temperatures of about 300 K at 110 GHz and 400 K at 220 GHz. The antenna half-power beamwidth and main beam efficiency were respectively $22''$ and 0.68 at 110 GHz, and $11''$ and 0.41 at 220 GHz. The observations were made in frequency switching mode. Linear baselines were subtracted from the observed individual spectra. The pointing accuracy was monitored frequently, and was found to be close to $3''$ rms.

The data were calibrated and analyzed with the GILDAS software developed at IRAM and Observatoire de Grenoble. Interferometric images were produced using natural weighting and cleaned in the usual way. The final resolution is $2.4'' \times 2.1''$ at position angle 75°. Fig. 1 presents a montage of the λ 2.7 mm continuum emission and of the $C^{18}O$, ^{13}CO and ^{12}CO (adapted from Gueth et al. 1996) J = 1 → 0 integrated emissions towards L1157.

Combination of the ^{13}CO J = 1 → 0 interferometric data and short-spacing informations provided by our single-dish observations was also performed (see Sect. 4), following a method described in Gueth et al. (1996).

3. Continuum emission

The λ 2.7 mm continuum emission consists in two distinct components. A compact source is found at $20^h39^m06^s.19$, 68°02′15″.9 (J2000.0), in good agreement with the previous observations at 115 GHz of Gueth et al. (1996). The flux density of this source is ∼ 35 mJy. In addition, low-level emission (1 to 3 mJy/beam) extended over ∼ $15''$ is detected around the compact source. Although weak, the signal level of this extended component is well above the noise rms (∼ 0.4 mJy/beam). The total flux of the continuum emission is ∼ 90 − 100 mJy. The spectral energy distribution of L 1157-mm is presented in Fig. 3 (see Sect. 3.3). The global shape of this distribution as well as the ratio between the submillimeter flux (radiated longwards of 350 μm) and the integrated flux match the definition criteria of the Class 0 protostars as defined by André et al. (1993).

3.1. Compact core

Because of the contribution of the extended component, deriving a size for the compact core is delicate. Using uniform weighting, we produced a map with a resolution of $2.1'' \times 1.4''$ at PA = 80°. In this map, the half-power contour is slightly elongated at PA = 70°, with a major axis size of $2.5''$, corresponding to a deconvolved size of $\simeq 1.3''$. We also performed a fit of a gaussian source directly into the visibility data, by using only baselines longer than 80 m. The formal result of this fit is an elliptical gaussian of total flux 35 mJy and size $1.24'' \pm 0.09'' \times 0.89'' \pm 0.06''$ at PA = 55° ± 8°, consistent with the previous determination from the map. At a distance of 440 pc, this corresponds to a linear size of about 550 × 400 AU. The derived position angle is nearly perpendicular to the outflow (PA ≃ 155°). Assuming optically thin emission, a dust temperature of 40 K, and a dust mass opacity of 0.01 cm^{2}g^{-1}, the inferred mass of the compact core is M ≃ 0.2 $M_\odot$. This mass could however be higher if the dust mass opacity is lower.

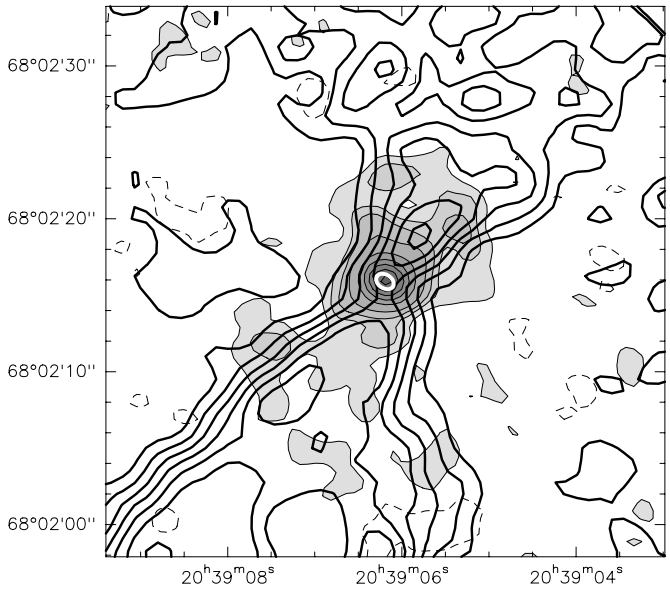

Fig. 2. Overlay of the λ 2.7 mm continuum emission (greyscale) and the integrated ^{12}CO J = $1 \rightarrow 0$ emission (thick contours). The contours are the same as in Fig. 1. The extended component of the continuum emission is clearly associated with the molecular outflow, and more precisely with the *edges* of the flow. The result of the fit of the compact core of the continuum emission (see Sect. 3.1) is drawn as a thick white ellipse.

3.2. Extended component

Due to its weakness and relatively large size, determination of the flux of the extended component is also difficult. The flux density measured on the shortest baseline (24 m) is 62 ± 3 mJy, but a 15″ source is already significantly attenuated on such baseline. The missing flux is partially recovered by CLEAN: the integrated flux in the whole clean map is 95 ± 10 mJy. The relatively high uncertainty is dominated by the difficulty to clean an extended, low surface brightness region. Nevertheless, we stress that the continuum emission of L1157-mm is actually dominated by its extended component, whose flux is 60 ± 10 mJy, almost two times higher than the flux of the compact core.

3.3. Model for the continuum emission

The compact source seen in the continuum emission map is elongated perpendicular to the outflow axis, has a linear size of $\sim$ 500 AU, and contains $\sim 0.2\ M_\odot$. Moreover, it lies exactly at the apex of the two collimated lobes of the molecular outflow (see Fig. 2). This strongly suggests that this component traces the protostellar L1157-mm condensation, possibly the accretion disk itself. The size of this compact core seems to be rather large compared to classical size of TTauri disks (e.g. Dutrey et al. 1996). Unfortunately, the angular resolution of the present observations is insufficient to study its inner structure.

The extended emission has a linear size of $\sim$ 6000 AU, and thus seems to arise from a large envelope surrounding the central object. At mm wavelengths, such envelopes have already been found to be necessary to explain observations of Class 0 objects (e.g. Terebey et al. 1993). In the case of L1157-mm, the observed morphology of the continuum emission compared to the CO outflow map (Fig. 2) suggests that most of the extended λ 2.7 mm emission actually comes from the part of the envelope which is disturbed by the outflow, and more precisely from the edges of the cavity excavated by the outflow. Such a weak continuum emission associated with the edges of the molecular outflow has already been observed in L 1551-IRS5 (Ladd et al. 1995), but at a higher frequency (λ 730 μm). Some published high-resolution maps of mm continuum emission in extremely young protostars also show marginally detected features along the edges of the associated flows (e.g. B335, Chandler & Sargent 1993; B5-IRS1, Langer et al. 1996; L1527, Ohashi et al. 1997).

Table 1. Parameters of the model shown in Fig. 3. The dust mass opacity κ_ν follows a law $\kappa_\nu \propto \nu^\beta$. The density and temperature are following $\rho(r) \propto r^{-p}$ and $T(r) \propto r^{-q}$ both in the envelope and in the layer, the maximal values corresponding to r = 440 AU, i.e. at the core boundary.

Core	temperature	36 K
	radius	440 AU
	mass	0.2 $M_\odot$
Envelope	max. temperature	20 K
	max. density (H_2)	$5{\cdot}10^6$ cm^{-3}
	radius	$\sim$ 5000 AU
	mass	$\sim$ 3 $M_\odot$
Layer	max. temperature	49 K
	max. density (H_2)	$5{\cdot}10^7$ cm^{-3}
	width	$\sim$ 200 AU
	mass	0.65 $M_\odot$
Dust opacity	β	1.0
	$\kappa(10^{12}$Hz)	0.1 cm^{2}g^{-1}
Density Law	p	1.0
Temperature Law	q	0.5

In order to investigate this configuration in more details, we have constructed a simple model of the dust emission, taking into account disturbances of an envelope by the effect of the outflow. We assumed that the dust distribution has three components: (1) A central condensation, modelled by a small and unresolved region of constant density and temperature (called "core" in Table 1). (2) A large spherical envelope, from which a cone of $\sim 30°$ opening angle has been emptied by the outflow. And finally, (3) a hotter and denser layer at the edges of the outflow conical cavity ("layer" in Table 1). Decreasing power-law distributions were used for the density and the temperature in both the envelope and the dense layer. The axis of the outflow and thus of the whole structure is inclined by 5° to the plane of the sky (Gueth et al. 1996). We then solved the radiative transfer problem by a simple step by step integration along the line of sight (see e.g. Dutrey et al. 1994).

We tried to model the continuum image at λ 2.7 mm and to reproduce simultaneously the spectral energy distribution (SED) of L1157. Parameters of the model are given in Table 1.

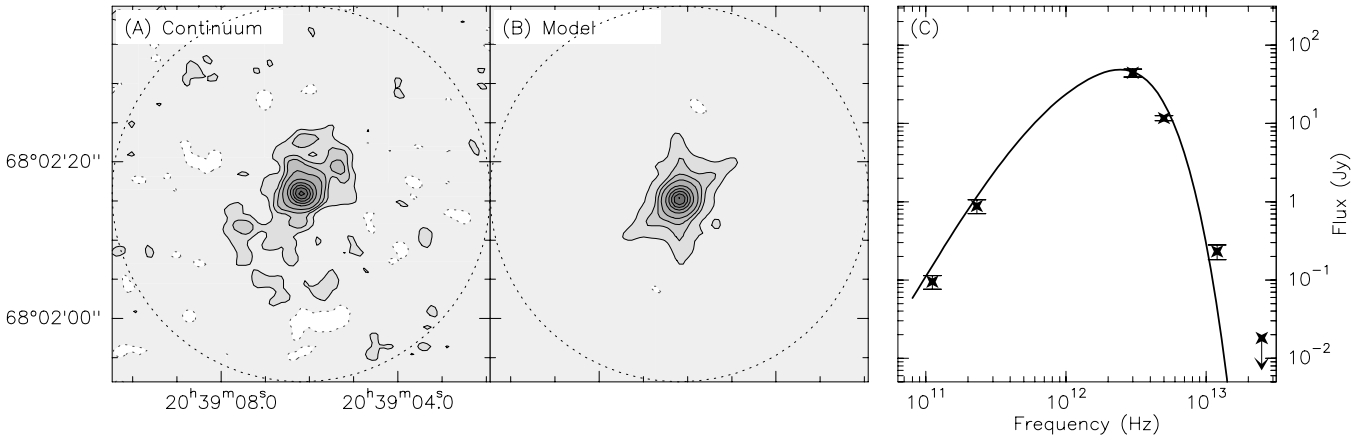

Fig. 3. a λ 2.7 mm continuum data (see also Fig. 1). **b** Simulated dust emission map at λ 2.7 mm. Contours are -1, 1, 2, 3, 5 to 30 by 5 mJy/beam for both the observations and the model. **c** Comparison between observed fluxes of L 1157-mm (crosses) and the modelled SED (continuous line). The 12 (upper limit), 25, 60, and 100 μm points are IRAS measurements (a color correction has been applied assuming the source is a 40 K black body: the only significant correction factor is the one used for the 12 μm point). The 1.3 mm flux (P.André, 1996, private communication) is a bolometer measurement performed at the IRAM 30-m telescope. Note that the flux density at 2.7 mm (these observations) is underestimated because it corresponds to interferometric data.

Fig. 3 is a montage of the λ 2.7 mm observations, the modelled image (after simulation of interferometric observations with the same uv coverage than the data and deconvolution) and the observed and modelled SED. The simulated image is in good agreement with the observations. It peaks on a central condensation of $\sim$ 40 mJy and presents extended features along the cavity edges on a scale of $\sim 15''$ with a total flux which agrees with the observational data. Three of the four small extensions of the simulated emission have corresponding features in the observations, while only an even more diffuse component is missing. Fig. 3 shows that the simulated SED also is in good agreement with the observed fluxes.

Given the simplicity of the model, the values given in Table 1 should be considered only as indicative. We note that in their modelisation of the continuum emission in L 1551-IRS5, Ladd et al. (1995) obtained a temperature ratio between the warm and cold components roughly similar to what we obtain here. However, our simulation points out that a temperature enhancement alone fails to reproduce the observed contrast in between the cavity edges and the unperturbed envelope. These observed features are reproduced only if there is also a steep increase of density inside the layer comparing to the density of the envelope (see Table 1). This yields an important mass (0.65 $M_\odot$) in this layer. In comparison, Ladd et al. (1995) only derived 0.02 $M_\odot$ for the similar feature in L 1551-IRS5. In the L 1157 case, the extended dust component is massive enough to be observed even at λ 2.7 mm.

A steep increase of density at the edges of the outflow is what is expected if the flow has pushed and compressed the medium in a dense layer along its edges. Our model is consistent with such a scenario since the mass of the dense layer is of the same order than the mass that would have been present in the empty conical cavity.

We also note that there is an order of magnitude between the derived mass of the central core ($\sim$ 0.2 $M_\odot$) and the mass of the whole envelope deduced from the model ($\sim$ 3 $M_\odot$). This last value is however not well constrained by the simulation. Moreover, the most extended part of the envelope remains unknown, since it is very faint and has also probably been filtered out by the interferometer. Nevertheless, the fact that most of the mass is in the envelope suggests that L1157-mm is still in its main accretion phase, which is one of the possible conceptual definitions of Class 0 sources (see e.g. André 1995).

4. Line emission

Integrated intensity maps of ^{12}CO, ^{13}CO, and C^{18}O emissions are presented in Fig. 1, together with the continuum map. Channel velocity maps are shown in Fig. 4 for C^{18}O and ^{13}CO, as well as for the ^{13}CO emission complemented by short-spacing (single-dish) observations.

4.1. C^{18}O *results*

The morphology of the C^{18}O emission resembles the continuum structure. The peak integrated intensity is 0.28 Jy.km.s^{-1}/beam, and the total integrated intensity is 0.9 Jy.km.s^{-1}. The peak brightness temperature of the C^{18}O emission is 6 K. If we correct for the source size measured using the continuum data ($1.3'' \times 0.9''$), the true brightness temperature reaches 25 K, which lies in the range of kinetic temperatures expected for such a condensation.

Assuming optically thin emission and a temperature of 40 K, the peak integrated intensity corresponds to a total mass for the central condensation of $4.7\,10^{-2}$ $M_\odot$ (for a standard molecular abundance: X(C^{18}O/H$_2$) = $1.4\,10^{-7}$). This is about 5 times lower than the mass of the central core derived from the

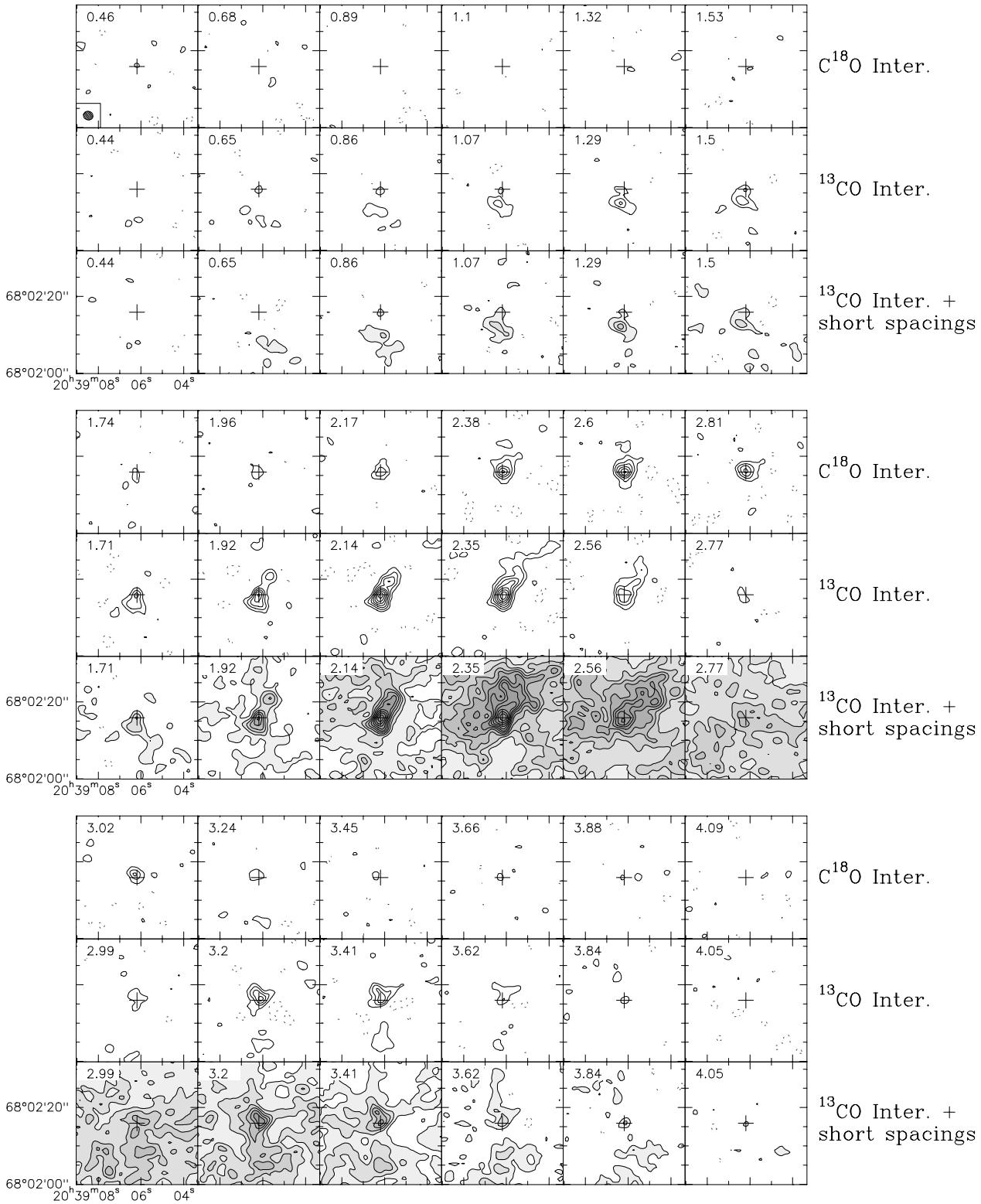

Fig. 4. Channel maps of the $C^{18}O$ (top row) and ^{13}CO (middle row) J = 1 → 0 emissions. The grey-scale maps (bottom row) are images of ^{13}CO J = 1 → 0 emission resulting from the combination of the single-dish and interferometric data. The central LSR velocity of each velocity interval is indicated at the upper left corner of each panel. First contour and step are 60 mJy/beam (1.1 K) for all maps. The noise level is ∼ 25 mJy/beam. The clean beam, indicated in the first channel, is $2.4'' \times 2.1''$ at PA = 75°. The systemic velocity of L 1157-mm is 2.6 km.s^{-1}.

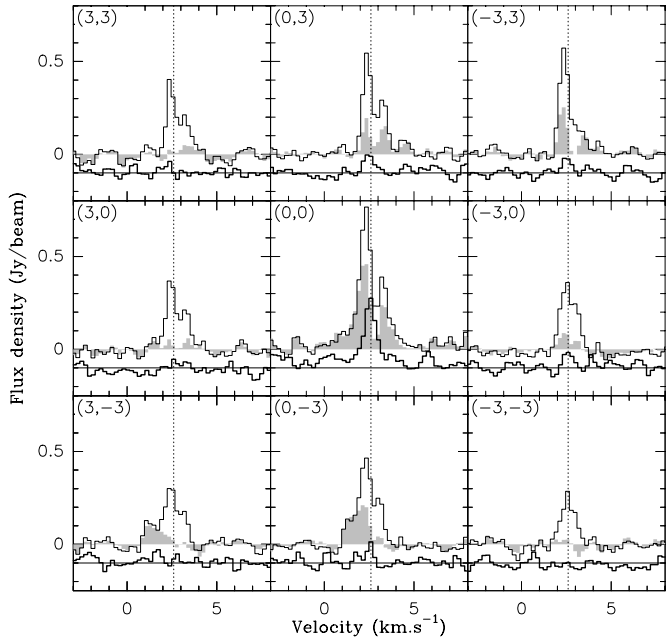

Fig. 5. ^{13}CO and C^{18}O profiles obtained around the L1157-mm central region. Offsets from the central position are indicated (in $''$) at the upper left corner of each plot. The shaded histograms are ^{13}CO profiles obtained from the interferometer data only, thin histograms are obtained with the addition of the 30-m data, and thick histograms are the C^{18}O spectra, shifted by -0.1 Jy/beam. The dashed vertical line indicates the LSR velocity of the C^{18}O core (2.6 km.s^{-1}).

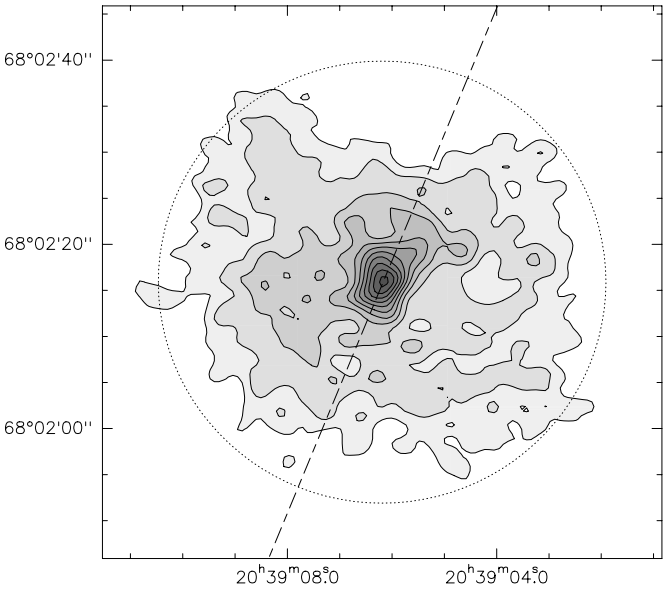

Fig. 6. ^{13}CO J = 1 → 0 interferometric + single-dish emission integrated between 2.1 and 3.4 km.s^{-1}, in order to avoid contamination by the high-velocity outflow. Contours are 0.15 to 0.65 by 0.05 Jy.km.s^{-1}/beam. The large-scale structure of the ^{13}CO emission is elongated in a direction roughly perpendicular to the outflow, whose axis is indicated by a dashed line. Note that this map has not been corrected from the interferometer primary beam (dashed circle) attenuation: the actual ^{13}CO emission extends over larger distances.

continuum data. Such discrepancies are found in more evolved objects (Class I & II, see e.g. Dutrey et al. 1996), but with a much larger magnitude. It is usually explained by CO depletion. In comparison, the rather small difference we obtain in the L 1157 case suggests that opacity and/or dilution effects alone could be at its origin. Hence, CO may not be significantly depleted in a Class 0 object as L 1157-mm (see also Langer et al. 1996, who derived similar conclusions for B5-IRS1).

Using the C^{18}O spectra, we find a systemic velocity of 2.60$\pm$ 0.05 km.s^{-1} for L 1157, slightly smaller than what was used by Gueth et al. (1996).

4.2. ^{13}CO *results*

The ^{13}CO and C^{18}O maps present a strikingly different aspect. When compared to the ^{12}CO emission (Fig. 1), ^{13}CO clearly delineates the edges of the molecular outflow, which is blue-shifted towards the South and redshifted towards the North. Since the L 1157 flow is nearly in the plane of the sky (Gueth et al. 1996), there is some red- and blue- shifted ^{13}CO emission on both sides of the flow.

Contrarily to the C^{18}O emission which peaks at V_{lsr} = 2.6 km.s^{-1}, the ^{13}CO emission is rather weak at this velocity, and almost inexistent in the two following channels of Fig. 4. It is however present at lower and higher velocities. This effect is better seen in Fig. 5, where we have superimposed the ^{13}CO and C^{18}O central spectra. The ^{13}CO profiles show at least three channels (2.6, 2.8 and 3 km.s^{-1}) in which proeminent self-absorption is present. It is noteworthy that these self-absorbed velocities are *redshifted*, as would be expected for an optically thick line in an infalling core with temperature decreasing outwards (e.g. Leung & Brown 1977).

4.3. Single dish ^{13}CO *results*

Fig. 4 also illustrates the importance of the single-dish ^{13}CO data to assess a complete picture of the region. The interferometer losses a fraction of the flux, since it filters out a large extended feature surrounding the central condensation. Fig. 6 presents the interferometric + single-dish integrated ^{13}CO emission.

When compared with the molecular outflow morphology traced by ^{12}CO (Fig. 1), the ^{13}CO emission appears elongated in a direction roughly perpendicular to the outflow. This suggests either that the large scale structure of the molecular core determines the direction of the flow, or that part of the envelope has already been disrupted or swept-up by the outflow.

Assuming optically thin ^{13}CO J = 1→0 emission, a lower limit of the total mass of the envelope is $\sim 1.4\ M_\odot$ (for T_{ex} = 20 K). This has to be compared to the mass of a few $M_\odot$ derived from the dust model (Sect. 3.3). However, optical depth effects are clearly important, since self-absorption features in the ^{13}CO spectra have been detected.

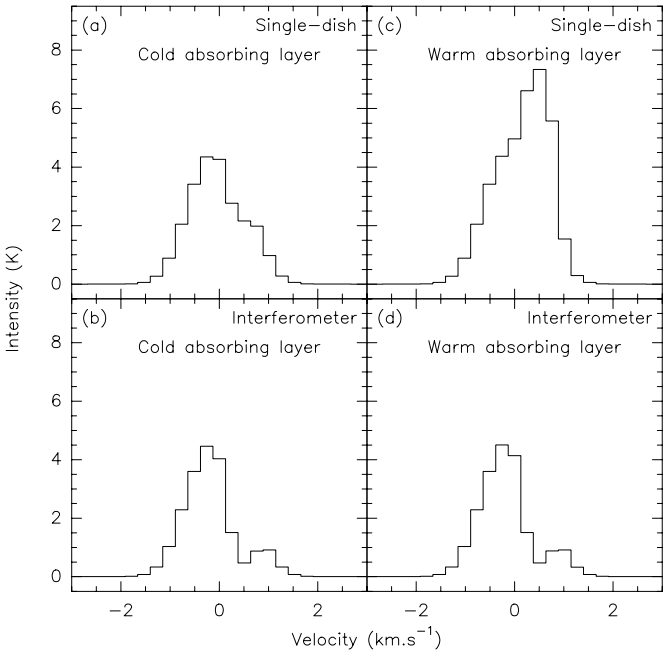

Fig. 7a–d. Synthetic profiles obtained from a centrally condensed core located behind an uniform, optically thick screen with a velocity shifted by +0.5 km.s^{-1}. **a** Single-dish profile obtained with a *cold* screen. **b** Corresponding interferometer profile. **c** Single-dish profile obtained with a *warm* screen. No self-absorption can be seen. **d** Corresponding interferometer profile showing "false" self-absorption.

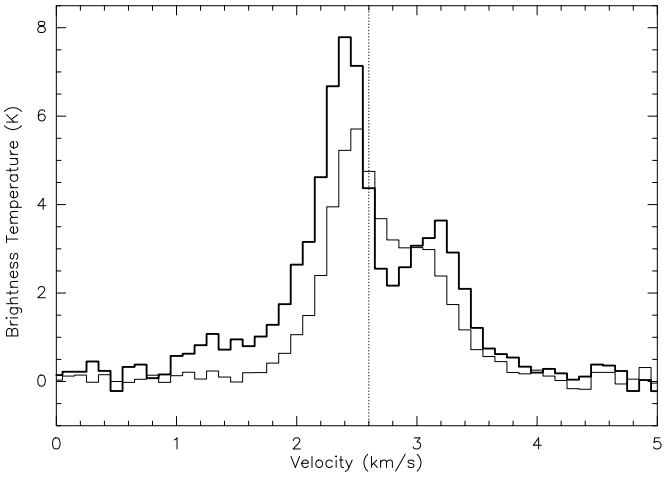

Fig. 8. Single-dish ^{13}CO J = 1 → 0 (thin histogram) and ^{13}CO J = 2 → 1 (thick histogram) spectra observed through the central position. The scale is in main-beam brightness temperature (T_{mb}). The beamwidth is 22″ at 110 GHz and 11″ at 220 GHz. The systemic velocity of L 1157 derived from C^{18}O is 2.6 km.s^{-1}, and is indicated as a dashed vertical line.

5. Gas kinematics

5.1. Interferometric observations of self-absorption

The deep self-absorption seen in the ^{13}CO profiles around the central condensation (Fig. 5) are redshifted with respect to the peak of the C^{18}O line by about 0.3 km.s^{-1}. Recently, similar self-absorption features have been detected with single-dish telescopes towards some other Class 0 protostars, and have been attributed to gravitational infall (e.g. Chandler & Sargent 1993; Zhou et al. 1993; Myers et al. 1995; Ward-Thompson et al. 1996). However, sensitivity limitations have made such infall self-absorption studies very difficult with mm-wave interferometers up to now. In the following, we would like to show that, contrarily to the single-dish case, the interpretation of such self-absorption features is not straightforward when observed with interferometers. Fig. 7 shows (left panels) results of simulations in which a centrally condensed core is obscured by an optically thick ($\tau \simeq 2$) uniform layer at lower temperature and different velocity (offset +0.5 km.s^{-1}). With a single-dish telescope, absorption is only slightly visible in the modelled profile (Fig. 7a), but when seen with an interferometer, it seems to be much more important (Fig. 7b). When the optically thick layer is warmer than the core (Fig. 7, right panels), emission from that layer is visible in the simulated profile (Fig. 7c) at 0.5 km.s^{-1}, but an interferometer would still see an *apparent self-absorbed profile* (Fig. 7d). This is because the interferometer resolves out the extended structure, whether it is absorbing or emitting.

Thus, pure interferometric data can be very misleading in drawing conclusions about self-absorption profiles. One actually needs to add short spacing information from a large single-dish telescope to avoid bias in the interpretation of the medium and large scale (i.e. $\sim 10''$) kinematics.

5.2. Is L1157-mm an infalling protostar ?

Since short-spacing information is crucial to study possible infall motions in protostellar cores, we have combined single-dish observations obtained at the IRAM 30-m telescope with the interferometric data of L1157. Figs. 4 and 5 show the resulting ^{13}CO J = 1 → 0 maps and spectra, in comparison with the purely interferometric data. The combined maps clearly confirm that the ^{13}CO self-absorption is real. It is present on a scale as large as $6 - 10''$, and could even be more extended, as suggested by single-dish ^{13}CO spectra (see Fig. 8). Such an extended self-absorption feature might in principle result from an unrelated foreground cloud, and a careful inspection of the data is necessary.

Fig. 9 shows higher resolution ($2.2'' \times 1.4''$) pure interferometric images obtained through "robust" (Briggs 1995) uniform weighting. These detailed maps show that the self-absorption feature is not structureless. Near V_{lsr} = 2.6 km.s^{-1}, the deepest self-absorption is just coincident with the peak of C^{18}O emission. Since the self-absorption dip peaks towards the central object, a chance coincidence with a foreground cloud becomes unlikely. Hence, it is quite tempting to interpret it as evidence for infall motion, despite the fact that the full kinematical pattern expected from an infalling envelope has not been revealed. In this case, a very crude estimate of the binding mass of $\simeq 0.6\,M_\odot$ can be made from the magnitude of the redshift and the extent of the self absorption, assuming free fall. This is larger than the

mass of the central condensation derived from the continuum emission.

A striking point is that the self-absorption is observed as a narrow lane, which drops very fast North and South of L1157-mm. The scale length in the N/S direction is resolution limited, i.e. less than 2″ or 900 AU at the distance of L1157 (see Fig. 9, channel at 2.56 km.s^{-1}). This seems to indicate that the self-absorbing medium is confined in a *flattened* structure, seen almost edge-on. The lack of sufficient background ^{13}CO emission a few arcsec away from the central source precludes studying the kinematical pattern on larger scales. The E/W size of this flattened infalling structure can thus hardly be properly derived from these observations, but seems to be at least 3 times its width.

We next try to obtain a rough estimation of the size of the infalling medium along the line of sight. Fig. 8 shows the single-dish ^{13}CO J = 1→0 and J = 2→1 spectra obtained through the central position. The self-absorption feature has a brightness temperature (in T_{mb} scale) of 3.2 and 2.2 K respectively. Assuming optically thick emission, this corresponds in both cases to an excitation temperature of $T_{ex} \simeq 6.3$ K. The self-absorption features are thus most probably sub-thermally excited, and then should be produced in a medium whose density is low enough to prevent thermalisation of the two lines. According e.g. to the LVG calculations of Goldsmith et al. (1983), the observed brightnesses of the two ^{13}CO lines are produced in a medium whose density $n(H_2)$ is $\sim 4.5\,10^3$ cm^{-3} (for a kinetic temperature of 10 K).

The pathlength L towards the central core is then given by: $L = \tau / (K\, n(H_2)\, m(H_2)\, \omega)$ where τ is the optical depth of the transition, $m(H_2)$ the mass of the H_2 molecule, ω the mean molecular weight, and K the mass absorption coefficient of the ^{13}CO J = 1→0 transition:

$$K = \frac{8\pi^3}{3h}\,\mu^2\,\frac{1-\exp\left(-\frac{h\nu}{k_B T_{ex}}\right)}{Q}\,\frac{1}{\Delta v}\,\frac{X(^{13}\mathrm{CO})}{m(H_2)\,\omega} \qquad (1)$$

μ is the dipole moment of ^{13}CO, Q the partition function, Δv the linewidth, and $X(^{13}\mathrm{CO})$ the abundance of ^{13}CO. Assuming normal ^{13}CO abundance (10^{-6}), $\Delta v = 0.3$ km.s^{-1} (approximate width of the self-absorption) and $\tau(^{13}\mathrm{CO}\ J = 1 \rightarrow 0) = 1$, a pathlength of about ∼ 8500 AU is obtained for $n(H_2) = 4.5\,10^3$ cm^{-3} and $T_{ex} = 6.3$ K.

This characteristic length for the infalling medium is roughly of the order of the radius of the envelope that surrounds L 1157-mm (see Sect. 3). Similar sizes have been found for other Class 0 objects (e.g. 7000 AU for NGC1333-IRAS2, Ward-Thompson et al. 1996; 5400 AU for L 1527, Zhou et al. 1996). It is however much larger than the 900 AU thickness derived from the self-absorption morphology. Although we reckon that these determinations are very uncertain because of low S/N, they seem to indicate that L 1157-mm is surrounded by a large flattened infalling structure, even more extended than what is suggested by the maps in Fig. 9, and seen almost edge-on. Such a flattened structure has a low probability to be seen edge-on, since its opening angle is lower than 10°. This is however coherent with the known inclination of the molecular outflow on the plane of the sky, which is ∼ 5° (Gueth et al. 1996).

We note that infalling motions cannot be detected through self-absorption profiles in a disk (or a flattened structure) which is not seen edge-on. As pointed by Saito et al. (1997), there is only one point in such a disk which has a given velocity along the line of sight, and no self-absorption is thus possible. To be observed, redshifted self-absorption requires an infall geometry in which several points have the same radial velocity, e.g. a spherically symmetric envelope or an edge-on disk, which is the case for L 1157-mm.

5.3. Rotation?

Since the central source of L1157-mm is extremely compact, the velocity pattern is unclear. However, the highest resolution images of the C^{18}O emission we have obtained (Fig. 9) suggest a small velocity gradient: the C^{18}O emission peaks about 2″ NE of the central core at V_{lsr} = 3 and 3.2 km.s^{-1}, while at 2.2 km.s^{-1} it is shifted ≃ 1″ West of the core. Since this gradient is roughly along the major axis of the compact continuum source, it could be indicative of rotation. From the measured displacement (∼ 3″) and velocity gradient (∼ 1 km.s^{-1}), and assuming keplerian rotation, one can roughly estimate a central mass of $\simeq 0.2\,M_\odot$, which is not inconsistent with the mass derived from the continuum emission.

We note however that this slight velocity gradient is not confirmed by the large scale (interferometric + single-dish) ^{13}CO images. The channel maps presented in Fig. 4 seem to indicate a general velocity gradient from NE (blueshifted emission) towards SW (redshifted), i.e. reversed with respect to the high resolution images.

6. Global structure of the L1157-mm vicinity

The continuum and spectral observations reported in this paper shed light on the gas and dust structure around a protostar like L 1157-mm. Outflow motions (traced by the ^{12}CO emission), gravitational infall (probably seen through the ^{13}CO self-absorption), and perhaps rotation (maybe seen as a velocity gradient in the C^{18}O map) seem to contribute to the kinematics of the protostar's vicinity. In addition, the continuum data indicate that temperature and density gradients are present in the region. The global picture emerging from our continuum and multiline study is summarized in Fig. 10. Schematically, a central object is surrounded by an infalling envelope, which could include a large flattened structure. The bipolar outflow has excavated a biconical cavity by pushing and compressing the matter, creating a dense hot layer between the envelope and the bipolar cavity. The resulting structure and kinematics are thus very complex.

The large flattened structure suggested by our observations could be the signature of a complex infall configuration. Recent theoretical models of protostellar collapses predict the formation of such flattened structures around the central condensation. For instance, Galli & Shu (1993) showed that the presence of a small magnetic field in the collapsing cloud can induce the

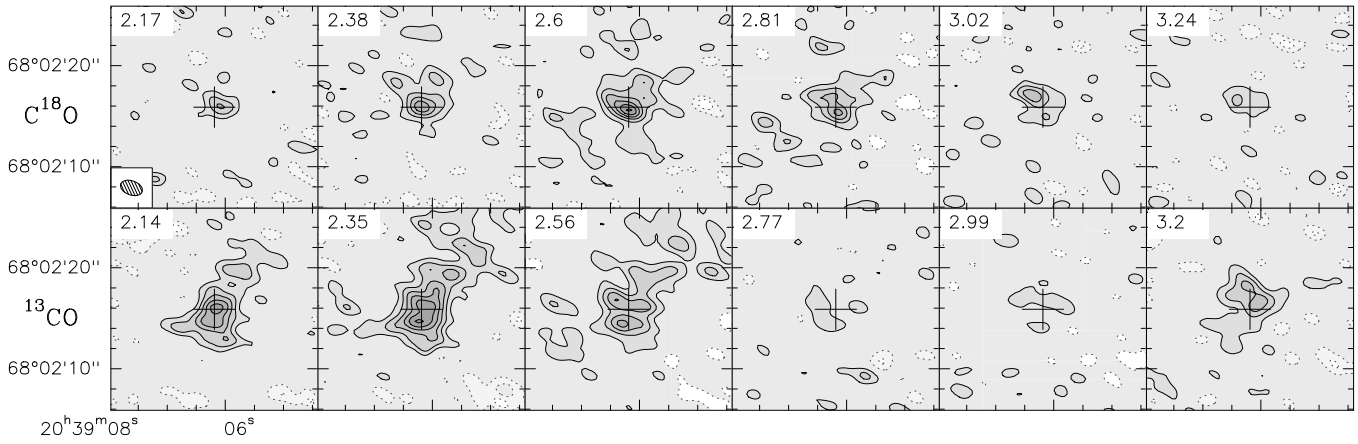

Fig. 9. Channel maps of the $C^{18}O$ J = 1 → 0 (top row) and ^{13}CO J = 1 → 0 (bottom row) emission obtained using uniform weighting. The beam size is $2.2'' \times 1.4''$ at PA = 69°. First contour and step are 50 mJy/beam, or 1.65 K.

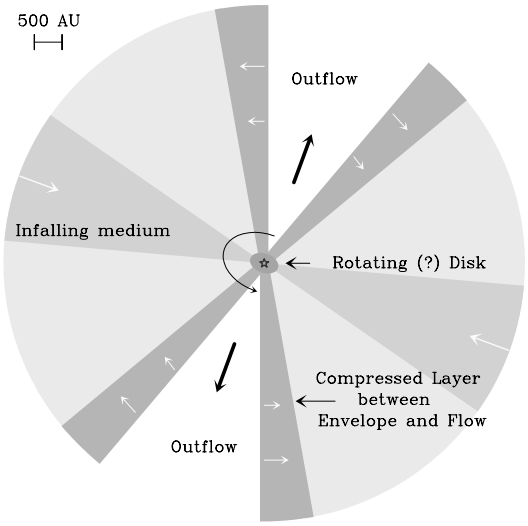

Fig. 10. General schematic view of the region around the L1157-mm protostar deduced from our continuum and mm line study (as viewed from the observer). The different components are a) an extended infalling envelope of $\sim 3\ M_\odot$, possibly including a large flattened component, b) a biconical cavity excavated by the outflow, c) a dense layer at the cavity walls consisting of $\sim 0.65\ M_\odot$ compressed by the outflow, and d) a dense dusty circumstellar structure (possibly a rotating disk) containing about $0.2\ M_\odot$.

formation of a "pseudo-disk", whose radius reaches a few thousands AU after a few 10^5 years. Hartmann et al. (1996) showed that a flattened distribution of the infalling gas is also obtained in the case of an initially flattened molecular cloud, which is likely to be common. Our observations are in qualitative agreement with these theoretical predictions, but do not yet allow to perform detailed comparisons.

7. Conclusions

The main conclusions of this paper are:

1.- We have marginally resolved the mm continuum emission of the Class 0 object L 1157-mm. The observed morphology is consistent with a large ($\sim$ 500 AU) flattened core, perpendicular to the outflow direction, possibly an accretion disk. The mass of this central object is $\sim 0.2\ M_\odot$, significantly lower than the estimated mass of the surrounding envelope ($\sim 3\ M_\odot$).

2.- Interaction between the collimated outflow and the envelope is an essential mechanism even in these very early stages of the protostellar evolution. The λ 2.7 mm continuum emission presents an extended component which arises from the heated and compressed edges of the outflow cavity.

3.- Strong indications for infall motions have been detected. High-resolution images and simple excitation considerations seem to indicate that the infalling medium is confined in a large flattened structure.

These results provide a quite detailed picture of the structure of Class 0 protostars. In fact, the first steps of the star formation process appear to be extremely rapid. Although L 1157-mm is still in its main accretion phase, a central condensation has already been formed, and even a rotating structure may be present. Hence, the disks which surround more evolved objects (e.g. Dutrey et al. 1996) could actually be created during the very first phases of the protostellar evolution.

The strong interaction between the molecular outflow and the envelope of the protostar as well as the presence of the outflow during the very first steps of the stellar formation show that the flow plays a crucial role in the mass assembling process. The outflowing and accreting phenomena are thus closely linked together. The precise understanding of the first phases of stellar formation requires to take into account the formation of complex accretion/ejection structures.

Acknowledgements. We are grateful to the IRAM staff at Plateau de Bure and Pico Veleta for competent help with the observations. We thank P.André for providing us informations prior to publication. We also thank F.Motte for many useful discussions. R.B. acknowledges partial support from Spanish DGYCIT Grant PB93-0048.

References

André P., Ward-Thompson D., Barsony M., 1993, ApJ 406, 122
André P., 1995, Ap & SS 224, 29
Avery L., Chiao M., 1996, ApJ 463, 642
Bachiller R., Martín-Pintado J., Fuente A., 1993, ApJ 417, L45
Bachiller R., Liechti S., Walmsley C.M., Colomer F., 1995, A & A 295, L51
Bachiller R., 1996, ARA & A 34, 111
Bontemps S., André P., Terebey S., Cabrit S., 1996, A & A 311, 858
Briggs D., 1995, PhD thesis, New Mexico Institue of Mining and Technology
Chandler C, Sargent A., 1993, ApJ 414, L29
Davis C.J., Eislöffel J., 1995, A & A 300, 851
Dutrey A., Guilloteau S., Simon M., 1994, A & A 286, 149
Dutrey A., Guilloteau S., Duvert G., et al., 1996, A & A 309, 493
Galli D., Shu F., 1993, ApJ 417, 243
Goldsmith P., Young J., Langer W., 1983, ApJS 51, 203
Gueth F., Guilloteau S., Bachiller R., 1996, A & A 307, 891
Guilloteau S., Delannoy J., Downes D., et al., 1992, A & A 262, 624
Hartmann L., Calvet N., Boss A., 1996, ApJ 464, 387
Hodapp K., 1994, ApJS 94, 615
Ladd E., Fuller G., Padman R., Myers P., Adams F., 1995, ApJ 439, 771
Langer W., Velusamy T., Xie T., 1996, ApJ 468, L41
Leung C., Brown R., 1977, ApJ 214, L73
Mikami H., Umemoto T., Yamamoto S., Saito S., 1992, ApJ 392, L87
Myers P., Bachiller R., Caselli P., et al., 1995, ApJ 449, L65
Ohashi N., Hayashi M., Ho P., Momose M., 1997, ApJ 475, 211
Saito M., Kawabe R., Kitamura Y., Sunada K., 1997, ApJ 473, 464
Tafalla M., Bachiller R., 1995, ApJ 443, L37
Terebey S., Chandler C., André P., 1993, ApJ 414, 759
Umemoto T., Iwata T., Fukui Y., et al., 1992, ApJ 392, L83
Ward-Thompson D., Buckley H., Greaves J., Holland W., André P., 1996, MNRAS 281, L53
Zhang Q., Ho P., Wright M., Wilner D., 1995, ApJ 451, L71
Zhou S., Evans N., Koempe C., Walmsley C., 1993, ApJ 404, 232
Zhou S., Evans N., Wang Y., 1996, ApJ 466, 296

This article was processed by the author using Springer-Verlag LaTeX A&A style file *L-AA* version 3.